

# Ball Grid Array Module With Integrated Shaped Lens for 5G Backhaul/Fronthaul Communications in F-Band

Aimeric Bisognin, *Student Member, IEEE*, Nour Nachabe, Cyril Luxey<sup>1</sup>, *Fellow, IEEE*,  
Frédéric Giancesello, *Member, IEEE*, Daniel Gloria,  
Jorge R. Costa<sup>2</sup>, *Senior Member, IEEE*, Carlos A. Fernandes<sup>3</sup>, *Senior Member, IEEE*,  
Yuri Alvarez<sup>4</sup>, *Senior Member, IEEE*, Ana Arboleya-Arboleya<sup>5</sup>, Jaime Laviada,  
Fernando Las-Heras, *Senior Member, IEEE*, Nemat Dolatsha, *Student Member, IEEE*,  
Baptiste Grave, Mahmoud Sawaby, *Student Member, IEEE*,  
and Amin Arbabian, *Member, IEEE*

**Abstract**—In this paper, we propose a ball grid array (BGA) module with an integrated 3-D-printed plastic lens antenna for application in a dedicated 130 GHz OOK transceiver that targets the area of 5G backhaul/fronthaul systems. The main design goal was the full integration of a small footprint antenna with an energy-efficient transceiver. The antenna system must be compact and cost effective while delivering an approximately 30 dBi gain in the working band, defined as 120 to 140 GHz. Accordingly, a  $2 \times 2$  array of aperture-coupled patch antennas was designed in the  $7 \times 7 \times 0.362$  mm<sup>3</sup> BGA module as the feed antenna of the lens. This achieved a 7.8 dBi realized gain, broadside polarization purity above 20 dB, and over 55% total efficiency from 110 to 140 GHz (20% bandwidth). A plastic elliptical lens 40 mm in diameter and 42.3 mm in height was placed on top of the BGA module. The antenna achieved a return loss better than  $-10$  dB and a 28 dBi realized gain from 114 to 140 GHz. Finally, active measurements demonstrated a  $>12$  Gbps Tx/Rx link at 5 m with bit error rate (BER)  $< 10^{-6}$  at 1.6 pJ/b/m. These results pave the way for future cost-effective, energy-efficient, high-data rate backhaul/fronthaul systems for 5G communications.

**Index Terms**—3-D printing, 5G, backhaul/fronthaul links, ball grid array (BGA), dielectric lens, millimeter-wave (mmw) antennas, organic module.

## I. INTRODUCTION

IN LESS than a generation, wireless communications and mobile data access have become essential features of

Manuscript received January 23, 2017; revised September 11, 2017; accepted September 15, 2017. Date of publication September 21, 2017; date of current version November 30, 2017. (*Corresponding author: Cyril Luxey.*)

A. Bisognin, N. Nachabe, C. Luxey, and A. Arboleya-Arboleya are with the University of Nice Sophia Antipolis, 06560 Valbonne, France (e-mail: cyril.luxey@unice.fr).

F. Giancesello and D. Gloria are with STMicroelectronics, 38920 Crolles, France.

J. R. Costa is Instituto de Telecomunicações, University of Lisbon, 1049-001 Lisbon, Portugal and also with the Instituto Universitário de Lisboa (ISCTE-IUL), 1649-026 Lisbon, Portugal.

C. A. Fernandes is with Instituto de Telecomunicações, University of Lisbon, 1049-001 Lisbon, Portugal.

Y. Alvarez, J. Laviada, and F. Las-Heras are with the University of Oviedo, 33203 Gijón, Spain.

N. Dolatsha, B. Grave, M. Sawaby, and A. Arbabian are with Stanford University, Stanford, CA 94305-4070 USA.

Color versions of one or more of the figures in this paper are available online at <http://ieeexplore.ieee.org>.

Digital Object Identifier 10.1109/TAP.2017.2755439

daily life. In the never-ending race to provide mobile users with greater data capacity, new wireless standards designed to achieve next-generation capacity and latency goals are emerging [1]. In this context, the 5G standard uses millimeter-wave (mmw) frequency bands to achieve the aforementioned goals of providing access to spatial degrees of freedom and beamforming gains [2]–[5]. To realize these capacity targets, urban small-cells (micro- and femtocells) need to replace macrocell base stations. Therefore, an important challenge lies in the transmission among these newly deployed small cells and between those base stations and the core network. Availability of cost-effective and energy-efficient solutions is of paramount importance in the final implementation of such 5G networks.

Wireless backhaul and fronthaul systems are possible alternatives to fiber-optic small-cell links [6]. Existing backhaul solutions operate in the *V*-band (57–66 GHz [7], [8]) and the *E*-band (71–76 and 81–86 GHz [9]–[11]) frequency range, but while they compete with fiber-optic links with respect to cost, data rates remain an issue [12] with an achievable limit of approximately 1–2 Gbps. This data rate range is insufficient for many 5G applications, which will require  $>10$  Gbps at 100 m or more by 2020 [4]. Another drawback of the available *V*- and *E*-band solutions is their high power consumption (20–35 W) attributable to the highly complex modulation schemes chosen for their spectral efficiency and interference mitigation.

All of these observations indicate that cost-effective, energy-efficient, high-capacity, and easy-to-deploy point-to-point wireless links at mmw frequencies are necessary for the proper deployment of 5G infrastructure. Since 2013, significant research has been conducted to find solutions in frequency bands above 100 GHz [13]–[17]. The wide bandwidth available in the *F*-band makes it possible to achieve data rates greater than 10 Gbps [13]. It should be noted that similar [14] and even higher data rates (up to 60 Gbps) [15] already have been demonstrated in the 140 and 240 GHz bands (25 Gbps) [16], [17], but complex modulation schemes are used in those solutions, which compromise energy efficiency. Operating above 100 GHz is interesting because it will enable

compact system solutions that can deliver Gbps data rates that compete with wired systems in many respects [18]. Further, the large frequency bandwidth available from 120 to 140 GHz allows relaxation of the spectral efficiency requirements and improves energy efficiency using an efficient modulation scheme. For mass-market deployment, we envision a compact system that is fully packaged with low-cost, flip-chip integrated circuits (ICs) on an organic substrate that includes antenna-in-package integration [19]–[21]. However, to increase the maximum operating distance, a higher gain is required than the one provided by a simple integrated antenna within a ball grid array (BGA) module. For this purpose, the BGA antenna was used as a feeding source of an integrated 3-D-printed lens to provide a small-footprint, fully integrated, cost-effective, 30 dBi antenna solution that overcomes traditional packaging challenges imposed at frequencies above 100 GHz.

In this paper, we propose a lens-integrated BGA module for 5G backhaul/fronthaul applications in the  $F$ -band (90 to 140 GHz). Section II describes the BGA module technology and the design of the source antenna for a dielectric lens. Section III presents the design and fabrication of the plastic lens. In the same section, the optimized dome lens is measured when fed by the BGA source. Section IV presents briefly the active measurements of a Tx/Rx system arrangement that demonstrates proof-of-concept results for a cost-effective, energy-efficient, 5G backhaul/fronthaul commercial solution. This paper ends with a conclusion and potential future improvements of the integrated system.

## II. BGA MODULE

To address the link requirements of potential 5G backhaul systems, an antenna that delivers approximately 30 dBi in the free-licensed 120–140 GHz frequency band was targeted. The approach selected to maintain a compact design was to employ a dielectric elliptical lens fed by a planar antenna source integrated within a low-cost BGA module that may yield an antenna gain that ranges from 20 to 35 dBi.

### A. $F$ -Band Antenna in BGA Packaging Technology

When fabricating feeding lines and antennas to operate above 50 GHz, an accuracy of tens of microns is required. Therefore, for the following reasons, the high-density interconnect (HDI) process [22], [23] was the technology selected to fabricate the source antenna.

- 1) A 50  $\mu\text{m}$  standard drawing rule (minimum conductor width and spacing between conductors) is available.
- 2) It is possible to select low-cost organic substrates with good performance above 50 GHz as build-up layers.
- 3) Automatic flip-chip assembly of the IC can be implemented, which is important considering an industrial approach and the target consumer mass market for 5G backhaul/fronthaul links [24].

Fig. 1 illustrates the integration scheme employed, which is of paramount importance at mmw frequencies [25]–[28]. The chip is connected in a “flip-chip” configuration to the BGA packaging using copper pillar technology (pad ring

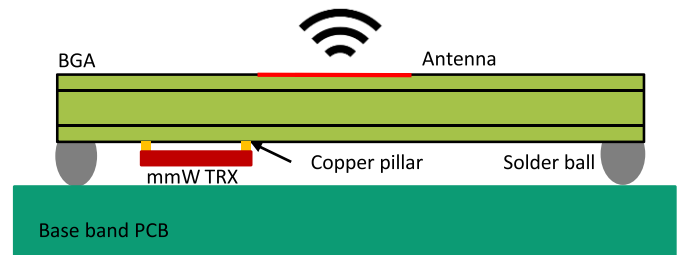


Fig. 1. Antenna-in-package integration scheme.

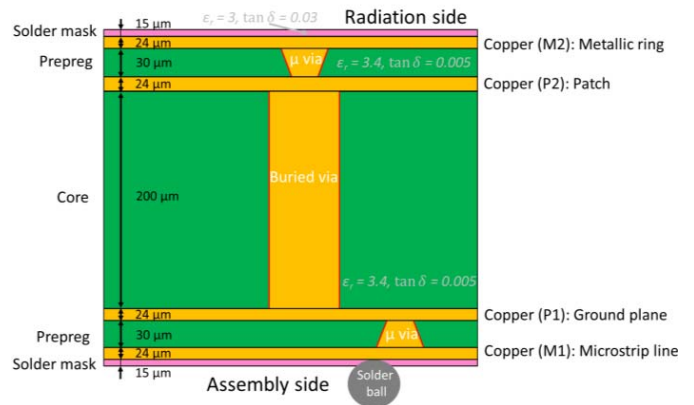


Fig. 2. Cross-sectional view of the 1-2-1 HDI build-up of the BGA module.

pitch  $< 150 \mu\text{m}$ ). The BGA is then connected to the PCB using solder balls with a 300  $\mu\text{m}$  diameter and 500  $\mu\text{m}$  pitch. The dc signals are routed from the PCB to the BGA through the solder balls and *ad hoc* routing lines are drawn on the BGA. The antenna is integrated into the multilayer BGA and radiates in the direction opposite to the chip, which minimizes the effect of the chip and PCB on the radiation of the antenna. This type of interconnection permits low-loss transmission between the RF output of the chip and the antenna.

It should be noted that several mmw antenna-in-package solutions [26], [29] have been published previously by prestigious academic and industrial researchers in various integration technologies such as PCB [30], Low temperature co-fired ceramic substrates [31]–[33], and organic/BGA assembly [34]–[42]; however, to date, we have found only one design that uses a BGA module that operates above 100 GHz [43].

The build-up layers of the BGA module are shown in Fig. 2. HDI technology imposes a symmetrical arrangement; thus, a standard 1-2-1 build-up consisting of 1 prepreg simple layer (30  $\mu\text{m}$ ), 1 core double layer (200  $\mu\text{m}$ ), and 1 prepreg simple layer (30  $\mu\text{m}$ ) was chosen. The core is made of a Mitsubishi CCL-HL972 substrate and the prepreg layers are made of Mitsubishi GHPL-970 substrate, both with  $\epsilon_r = 3.4$  and  $\tan \delta = 0.005$ . The 15  $\mu\text{m}$ -thick solder mask is made of TaiYo AUS410 with  $\epsilon_r = 3$  and  $\tan \delta = 0.03$ . All copper layers are 24  $\mu\text{m}$  thick. As Fig. 2 indicates, the dc lines are drawn at M1 (chip and PCB side), as well as the microstrip line. The ground plane is set at P1. Both prepreps were protected by a 20  $\mu\text{m}$  thick solder mask. The chip was assembled using standard industrial procedure. Consequently, standard underfill

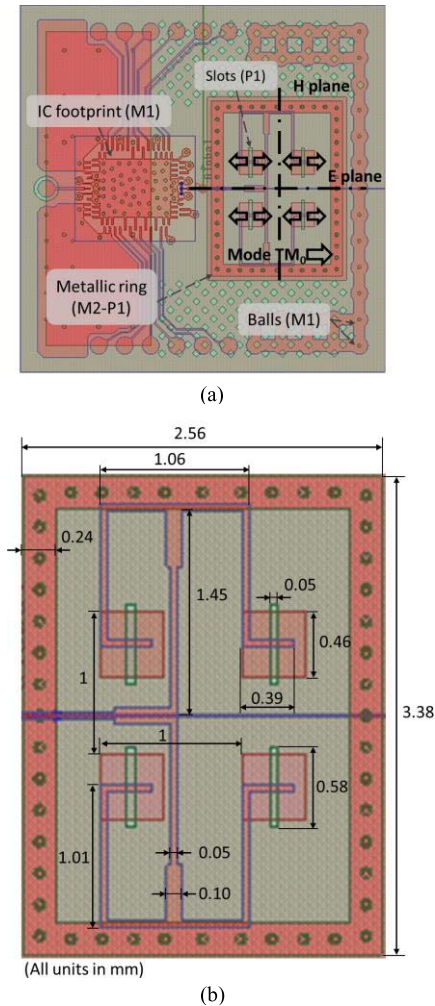


Fig. 3. Transparent view of all layers of the BGA module. (a) Bottom view of the module with IC footprint and coupling slots fed by microstrip lines, with indications of the direction of propagation of  $TM_0$  mode generated by the slots. (b) Detailed view and dimensions of the  $2 \times 2$  array of slot-fed patches and feeding line of the module.

was used in this assembly, and was taken into account in the electromagnetic simulation of the module.

The dimensions of the BGA module are  $7 \times 7 \times 0.362$  mm<sup>3</sup>. Figs. 3 and 4 show a transparent view and the top and bottom views of the BGA. Fig. 3(b) shows a detailed view of the antenna together with the main dimensions of its components.

The BGA module integrates a specially designed  $2 \times 2$  array of four aperture-coupled patch antennas. Each patch in the array is coupled to a microstrip-fed resonant slot to maximize the matching and gain bandwidth. The thickness of the prepreg substrates was minimized to increase the coupling between the microstrip line and the slot, and took into account the minimum resolution of the HDI technology ( $50 \mu\text{m}$ ). The slots were set at level P1 and the patches at P2. The  $200 \mu\text{m}$  thickness of the core was chosen to meet the target bandwidth (120 to 140 GHz). A 1:4 microstrip divider divides the power equally among all patches and is characterized by an input impedance close to  $50 \Omega$ . Fig. 3(b) shows that the total length of the signal path (transmission lines) in the power divider is approximately 4.5 mm, yielding a total simulated

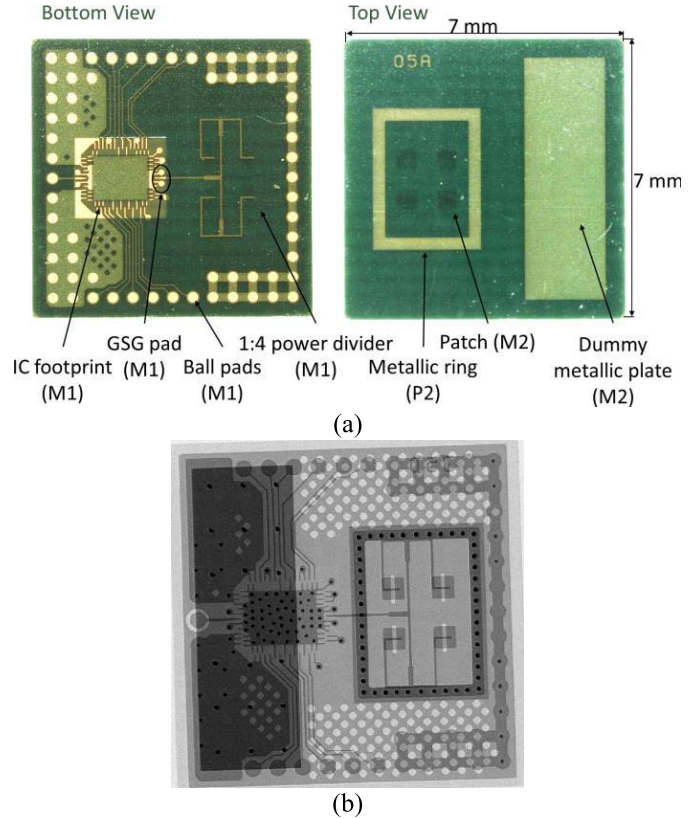


Fig. 4. (a) Photographs of bottom and top view of the BGA module integrating the  $2 \times 2$  antenna array. (b) X-ray of the BGA module.

loss of 1.1 dB at the center frequency of the working band. The spacing between the patches was adjusted to obtain optimal illuminating beamwidth for the elliptical lens chosen: 1 mm (corresponding to  $0.43 \lambda_0$  at 130 GHz) in both the  $x$ - and  $y$ -transverse directions. The goal was to obtain a Gaussian radiation pattern in both the E- and H-planes of the BGA module with a level  $-10$  dB below the maximum within an  $80^\circ$ – $100^\circ$  angular region. This particular element arrangement was chosen because it cancels in part the  $TM_0$  surface wave modes generated by the slots within the core substrate from out-of-phase natural recombination. In addition, the array antenna was surrounded by a grounded metallic ring to collect and radiate the residual energy from the  $TM_0$  mode with the main radiation of the array antenna.

### B. BGA Module Performance in Air

To validate the design within the HDI technology, the BGA module radiating into air was probe-fed and measured with the customized 3-D measurement range presented in [44], and extended to the  $F$ -band with mmw extenders [45]. As shown in Fig. 5, the measured reflection coefficient largely was consistent with simulated results: the  $|S_{11}|$  was less than  $-10$  dB from 96 to 140 GHz. The wide bandwidth achieved is attributable to the complementary behavior of the slot, the patch, and the metallic ring surrounding the array antenna. The main discrepancies between the simulation and measurements occurred because the probe and some of the elements of the BGA, such as the IC dc traces, the dummy plates, and

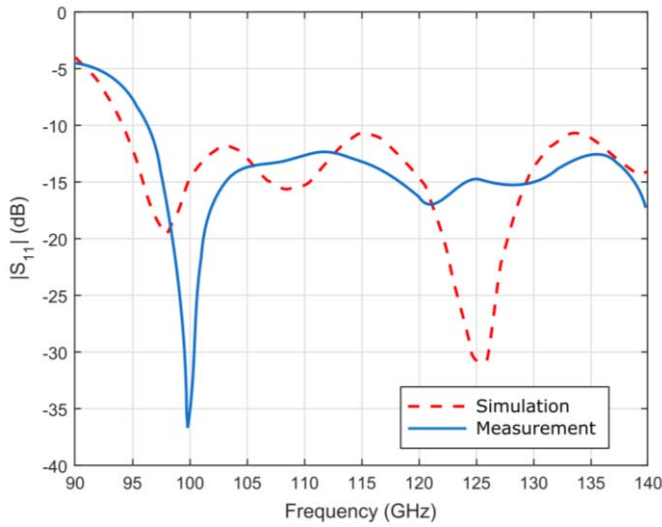


Fig. 5. Simulated and measured  $|S_{11}|$  of the array antenna of the BGA module radiating in air.

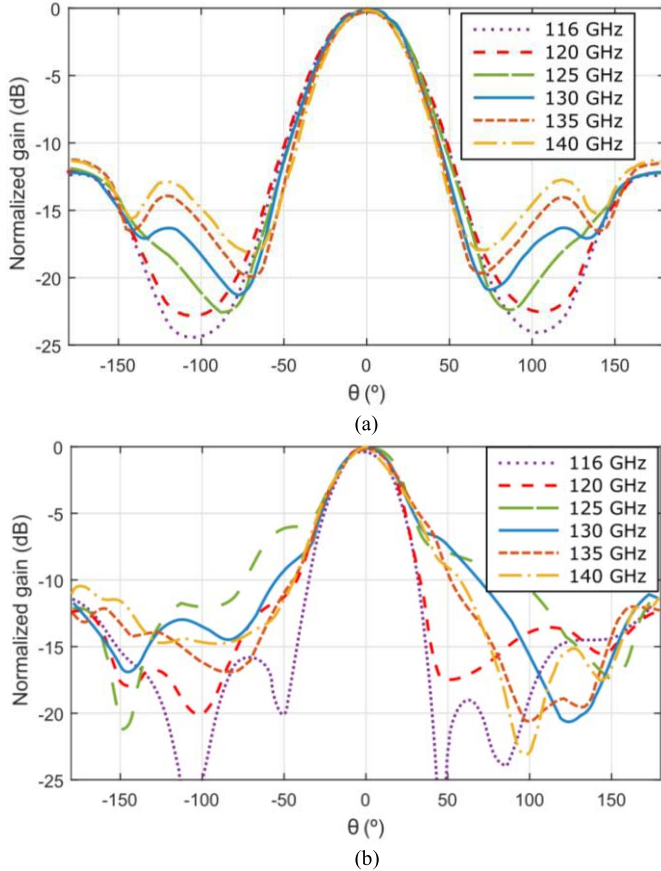


Fig. 6. Simulated normalized E- and H-plane radiation patterns of the array antenna of the BGA module radiating in air from 116 to 140 GHz. (a) H-plane ( $\varphi = 0^\circ$ ). (b) E-plane ( $\varphi = 90^\circ$ ).

the ball pads (which could not be taken into account during the simulations), affect the measurements.

Fig. 6 presents the simulated radiation patterns in the E-plane ( $\varphi = 90^\circ$ ) and H-plane ( $\varphi = 0^\circ$ ) at several frequencies within the band of interest. A quasi-constant beamwidth

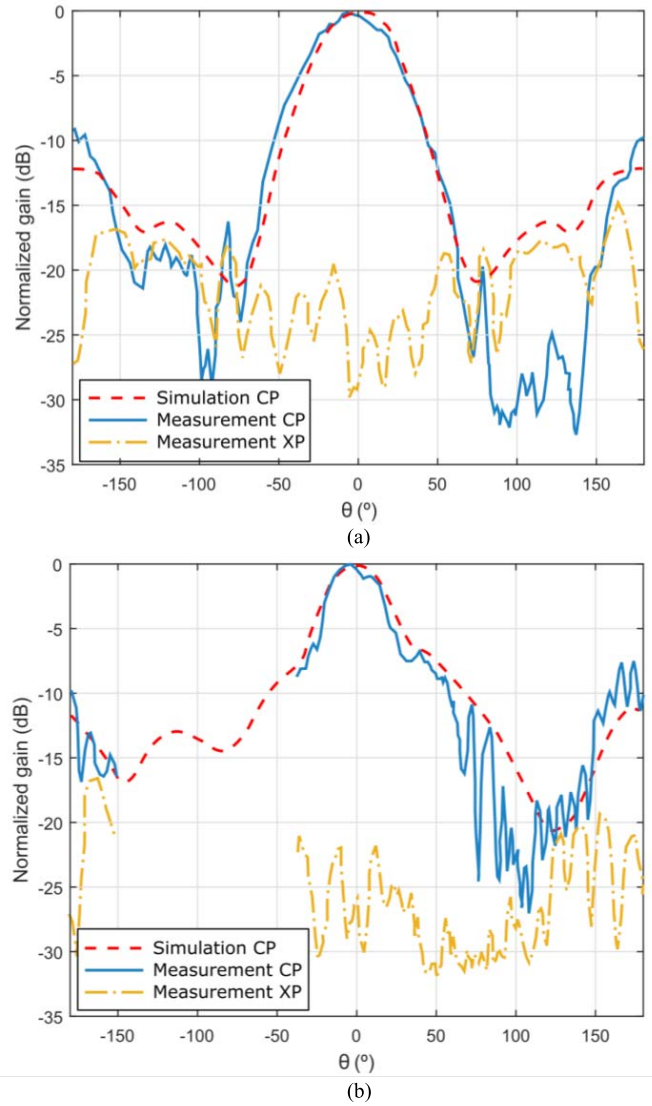


Fig. 7. Simulated and measured realized gain radiation pattern of the array antenna of the BGA module radiating in air at 130 GHz. (a) H-plane ( $\varphi = 0^\circ$ ). (b) E-plane ( $\varphi = 90^\circ$ ).

of  $88^\circ$  at  $-10$  dB was maintained from 116 to 140 GHz in the H-plane (in fact from  $84\text{--}96^\circ$ ). However, a stronger variation was noted in the E-plane despite careful optimization of the metallic ring for  $TM_0$  surface-wave mode management. A comparison between the simulated and the realized gain measurements of the E- and H-planes radiation patterns at 130 GHz is presented in Fig. 7. Very good agreement was observed in the H-plane. Except for the masking effect of the probing system that occurred in the E-plane and prevented measurements in the range from  $-150^\circ$  to  $40^\circ$ , the agreement between the simulation and the measurement remained acceptable in this plane. The beamwidth measured at  $-10$  dB (relative to the maximum gain) was  $90^\circ$  in the H-plane and approximately  $110^\circ$  in the E-plane. The simulated Front-to-Back ratio (F/B) was 12.5 dB, while that measured was 10 dB; therefore, the fractional power delivered to feed the lens was  $\sim 90\%$ . The broadside cross-polar level was below  $-25$  dB in both planes and below  $-15$  dB in the backside direction of the BGA module.

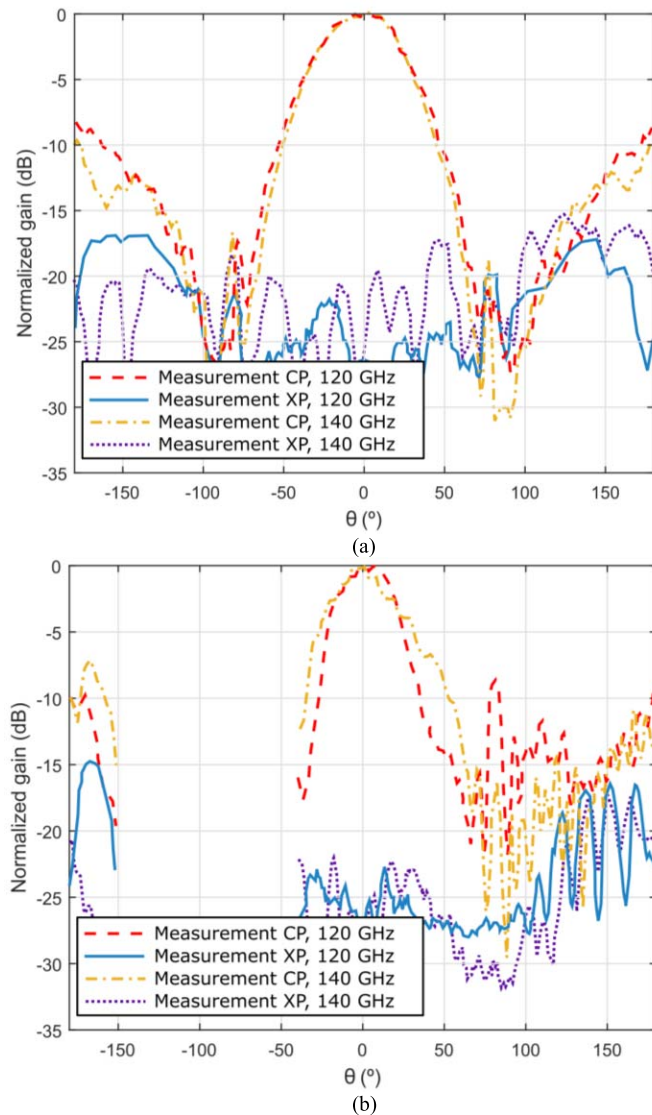


Fig. 8. Measured realized gain radiation pattern planes in the extremes of the working band of the array antenna of the BGA module radiating in air. (a) H-plane ( $\varphi = 0^\circ$ ). (b) E-plane ( $\varphi = 90^\circ$ ).

Fig. 8 shows the normalized realized gain for the main cuts at the extremes of the frequency band: 120 and 140 GHz. The measurement results exhibited good agreement with the simulations of BGA behavior depicted in Fig. 6. Fig. 9 shows the simulated and measured realized gain in the broadside direction of the top face of the BGA module. The simulated realized gain varied between 9 and 10 dBi from 116 to 140 GHz, and the measured realized gain values were very close to those simulated (above 7.8 dBi in the working band at minimum). Note that the uncertainty of the measurement setup [44], [45] was  $\pm 1.2$  dB at 140 GHz. The broadside polarization purity was greater than 20 dB along the  $F$ -band. It is very interesting to notice the gain flatness and a total simulated efficiency greater than 66% within the working band, defined as 120 to 140 GHz.

The hybrid method described in [46] has been employed to compute the efficiency measured. This method combines

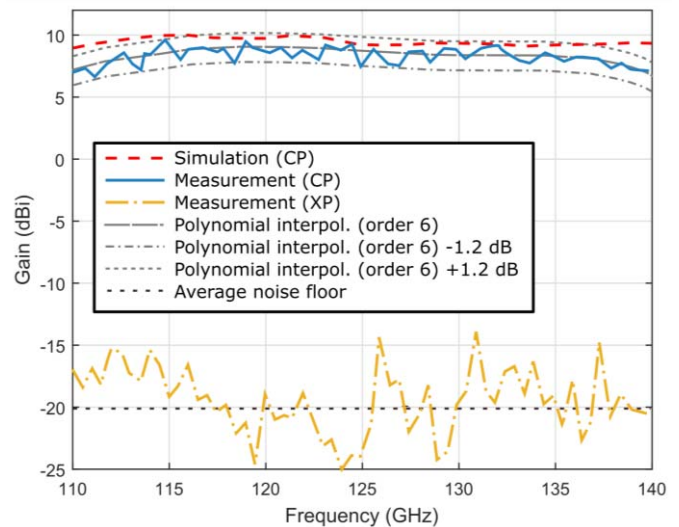


Fig. 9. Simulated and measured broadside realized gain (co- and cross-polarizations) versus frequency of the BGA array antenna.

a quasi-3-D acquisition of the realized gain radiation pattern (representing 73.5% of the surface of the sphere), with simulation data in the region in which the radiated field cannot be acquired because of the mechanical restrictions of the setup (see Fig. 16). The total efficiency measured was estimated to be 55% at 130 GHz. Therefore, considering that 90% of the power radiates toward the lens, 49.5% of the input power to the source is used to feed the lens.

All of the air measurements of the BGA module validated the HDI technology and the build-up chosen for an efficient 120–140 GHz planar source for an elliptical dielectric lens. The next step was to design an elliptical lens illuminated by this array-antenna source.

### III. LENS DESIGN

#### A. ABS Material

As the target design was a cost-effective antenna system for mass-market production, the use of 3-D printing technology and adequate materials for the fabrication of the elliptical lens were evaluated next. Usually, above 60 GHz, quartz material [47], [48] or high-density polyethylene [49] is used for mmw lenses. However, these materials are expensive and require dedicated tooling. Therefore, the method chosen was fused deposition modeling (FDM) using ABS-M30 plastic. To the authors' best knowledge, ABS-plastic has been used rarely to date to design/fabricate an antenna that operates at frequencies above 100 GHz [50]; however, several attempts have been made at lower frequencies [51]. The FDM 3-D printing technology relies on the deposition of a thin plastic filament to build layers in an additive manufacturing process. In our case, the in-house machine was able to deliver an ABS-M30 plastic filament with a diameter of  $178 \mu\text{m}$ . This kind of plastic is used frequently for the casing of common communication devices (e.g., smartphones, cameras, laptops).

A dielectric lens made of this plastic can focus the waves originating from the planar BGA source in a narrow

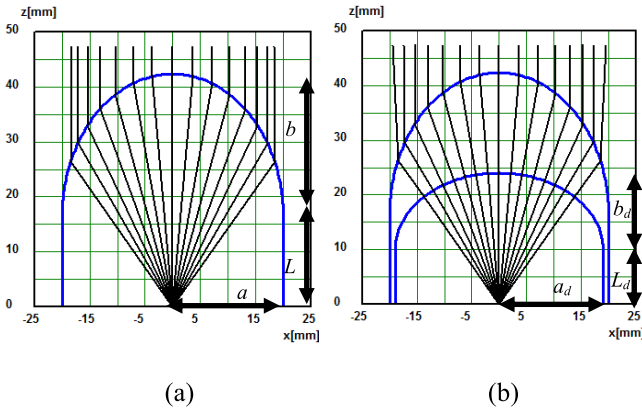


Fig. 10. (a) Profile and ray tracing of an integrated elliptic lens in ABS material. (b) Profile and ray tracing of a dome-type integrated elliptic lens in ABS material.

radiated beam. At the same time, it also can serve as part of the casing of the backhaul system. In this way, the radome casing's negative effect on the performance of the antenna is minimized while a low-cost system design is achieved.

The method described in [52] was implemented to extract the complex permittivity of the ABS-M30 in the 110–125 GHz band, and the value computed was  $\epsilon_r = 2.49 - j0.027$ . A quasi-optical method developed at ESA/ESTEC [53] also was used to extract the permittivity at 137.5 GHz, and a value very close to the previous one was found:  $\epsilon_r = 2.48 - j0.025$ .

### B. ABS Elliptical Lens

As mentioned previously, the target gain of the antenna of the full system for 5G backhaul links at 130 GHz (central frequency of the working band) was set at approximately 30 dBi. This high gain can be achieved by adding an integrated 3-D-printed dielectric lens on top of the BGA module that is used as a primary feed. A simple single-material lens configuration that simultaneously maximizes the achievable gain is the elliptical lens [54]. The elliptical lens [see Fig. 10(a)] was defined here as a half ellipsoid with radius  $a$  along the  $x$ -axis, and a cylindrical extension  $L$  from the feed to the center of the ellipse. The ellipse radius along the  $z$ -axis is  $b$  [54]

$$b = \frac{a}{\sqrt{1 - 1/\text{Real}(\epsilon_r)}} \quad (1)$$

$$L = b/\sqrt{\text{Real}(\epsilon_r)}. \quad (2)$$

The radius  $a$  should be chosen according to the target directivity in dB, which can be estimated from

$$\text{Dir[dB]} = 20\text{Log}_{10}(2\pi a/\lambda) \quad (3)$$

where  $\lambda$  is the operating wavelength. However, the dielectric material dissipation losses in the lens, which can be estimated by (4) [55], affect the gain

$$\text{Loss[dB]} = 27.3\sqrt{\text{Real}(\epsilon_r)}(L + b)\tan\delta/\lambda \quad (4)$$

where  $L + b$  is the lens height at the axis and the loss tangent is  $\tan\delta = -\text{Imag}(\epsilon_r)/\text{Real}(\epsilon_r)$ .

Disregarding for now the efficiency of the array antenna (BGA) radiation, the lens base radius should be

chosen so that Dir-Loss is  $\sim 30$  dB. For a low-cost material, such as ABS ( $\epsilon_r = 2.48 - j0.0248$ ), which is compatible with FDM 3-D printing, choosing  $a = 20$  mm provides a directivity of  $\sim 34$  dBi. Using (1) and (2), the other lens dimensions become  $b = 25.89$  mm and  $L = 16.44$  mm. Then, the dissipation loss estimated from (4) is 7.3 dB. Therefore, the lens' directivity needs to be increased. One possibility is to increase the overall size of the lens, i.e., increase the radius,  $a$ . However, in doing so, the dissipation loss also increases. A much more elegant and efficient approach is to optimize a dome-type elliptical lens with air below it to reduce the dissipation losses without reducing the focusing capability and, consequently, directivity. The simplest dome configuration would have a spherical surface at the feed side with a radius of  $a_d$  that is centered at the array antenna of the BGA module. Because one must ensure that there is a lateral wall of ABS material to attach the IC to the lens, the maximum value for the radius would be  $a_d = 19$  mm with a 1 mm thick lateral wall. This would reduce the dissipation path length inside the ABS material to  $L + b - a_d = 23.33$  mm.

To achieve even greater reduction of the path length inside the ABS material, the lower surface of the dome can be elliptical instead, with a base radius of  $a_d$  along the  $x$ -axis, a radius of  $b_d$  along the  $z$ -axis and a cylindrical extension,  $L_d$  [see Fig. 10(b)]. However, this will cause the radiation from the array antenna to be refracted at the dome's elliptical surface. Therefore, to ensure that the lens does not lose directivity, the dome parameters must be optimized. Using the Genetic Algorithm routine in the ILASH tool [56], those optimized dome parameters were  $a_d = 19$  mm,  $b_d = 14$  mm, and  $L_d = 10$  mm. As can be seen in Fig. 10, the ray tracing of both the full lens and the dome lens present a collimation effect with exiting rays almost parallel to the lens axis. With this dome lens, the height of the ABS material in the lens was reduced to  $L + b - L_d - b_d = 18.33$  mm, and by using (4), the dissipation loss was now estimated to be 3.2 dB. The advantages of this dome lens were confirmed by performing a full-wave simulation in HFSS software. Fig. 11 compares the results to a full (material) elliptical lens. Gain is represented versus  $a$  radius, where the dome radius is  $a_d = a - 1$  mm. It is clear that for larger lenses, the proposed dome configuration is very advantageous. In fact, there is an optimal radius for the full ABS-M30 lens, because increasing the lens radius further does not increase the gain, but on the contrary, reduces it because of higher dissipation losses, as shown in Fig. 11.

### C. Fabrication and Measurements of the Dome Lens

To measure the performance of the quasi-optical antenna of the full system composed of the BGA source and the elliptical dome lens, a thin plastic support was designed specially. To place the BGA module accurately at the focal point of the lens, a small cavity the size of the BGA module was included in the design [see Fig. 15(a)]. The support and the dome lens were realized separately by FDM 3-D printing and then attached together using the rotating fin mechanism shown in Fig. 12(a).

The overall optimized dimensions of the dome lens are shown in Fig. 12(b). The thickness of the support for the

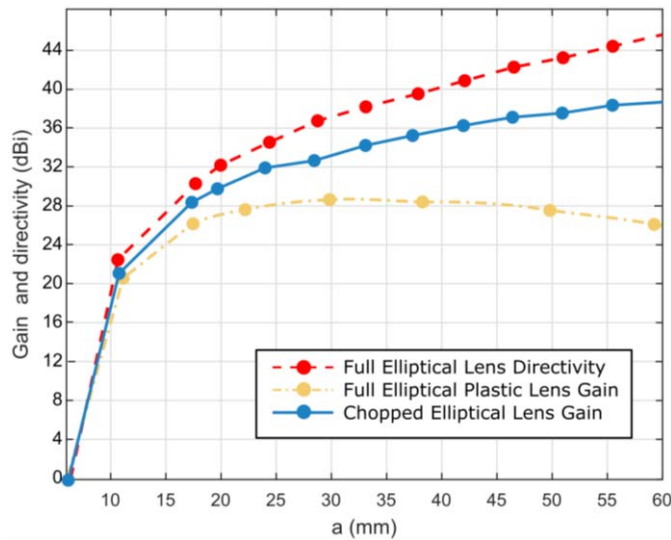
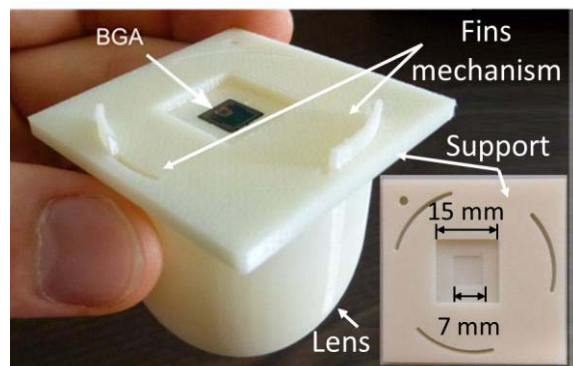
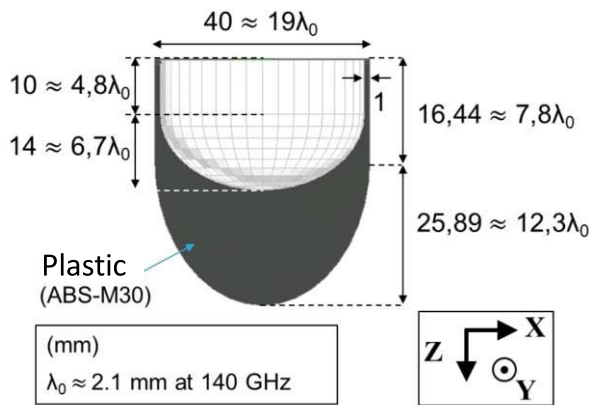


Fig. 11. HFSS full-wave simulations of the directivity and gain of a full elliptical lens and a dome elliptical lens (called chopped) of ABS-30 material versus the lens base radius  $a$  at 130 GHz.



(a)



(b)

Fig. 12. Description of the elliptical dome lens with BGA source. (a) Photograph of the assembly scheme. (b) Overall dimensions of the dome lens.

BGA cavity was optimized to achieve optimal illumination of the dome lens from the source antenna. An HFSS simulation model was elaborated and a parametric study was conducted to determine the best thickness  $t$  (see Fig. 13).

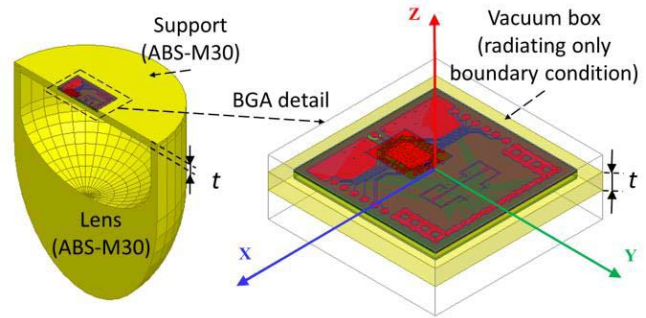


Fig. 13. HFSS 3-D view of the dome lens antenna (left). HFSS model (right) of the BGA source radiating into an ABS-M30 plastic support of thickness  $t$ .

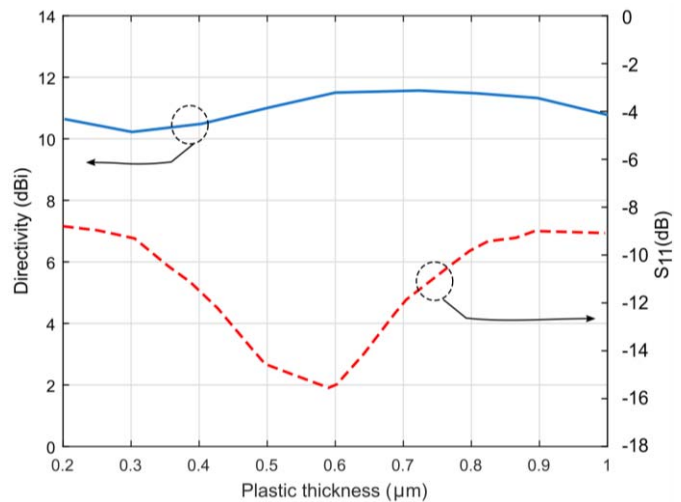


Fig. 14. Directivity in the broadside direction (plain line) and reflection coefficient  $|S_{11}|$  (dashed line) of the HFSS model versus the plastic support thickness  $t$  at 130 GHz.

The best performance was found at  $t = 600 \mu\text{m}$ , giving a  $|S_{11}| < -16 \text{ dB}$  and a BGA module directivity of approximately 11 dBi in its broadside direction (Fig. 14). For this selected thickness  $t$ , Fig. 15 shows the main cuts of the normalized radiation pattern of the array antenna radiating into the plastic support at 130 GHz. Those simulated patterns were compared to simulated patterns of the BGA source radiating into air, and showed no significant disturbance in the H-plane, but beneficial differences in the E-plane where, interestingly, the  $-10 \text{ dB}$  beamwidth was reduced. The beamwidth at  $-10 \text{ dB}$  (relative to the maximum directivity) was  $80^\circ$  in both planes, and the side lobes levels were less than  $-15 \text{ dB}$  in the H-plane, and  $-10 \text{ dB}$  in the E-plane.

The next step was to measure the input matching and the radiation pattern of the full antenna system. Fig. 16 shows the employed antenna measurement setup. The measured  $|S_{11}|$  with microelectronic probing revealed  $-10 \text{ dB}$  impedance matching from 114 to 140 GHz and possibly more (20% bandwidth: see Fig. 17). The setup allowed measurement distances from 20 to 60 cm up to 140 GHz. Taking into account the size of the dome lens ( $D = 40 \text{ mm}$ ), the far-field (FF) distance was  $R_{\text{FF}} = 1.5 \text{ m}$  at  $f = 140 \text{ GHz}$ , indicating that near-field (NF) acquisitions and a NF to FF (NF-FF) transformation are required to obtain the FF radiation patterns.

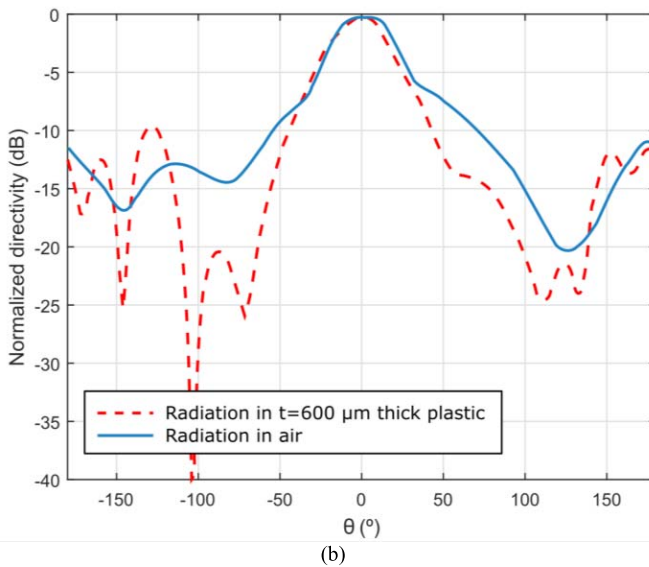
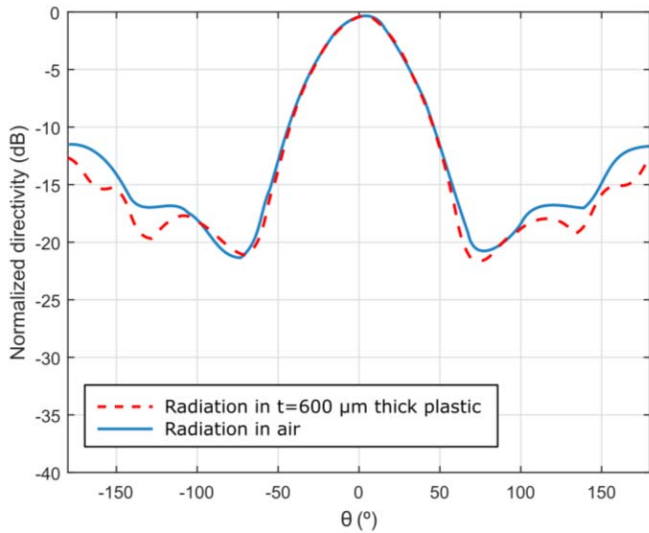


Fig. 15. Simulated normalized radiation patterns of the BGA module radiating through the support thickness of  $600 \mu\text{m}$  (dashed lines) and in the air (plain lines) at 130 GHz. (a) H-plane ( $\varphi = 0^\circ$ ). (b) E-plane ( $\varphi = 90^\circ$ ).

Positioning accuracy and thermal stability requirements of the *F*-band are very demanding and increase the cost and complexity of the measurement setup. Thus, for this purpose, phaseless techniques are more suitable (and realistic) than are complex field acquisitions with amplitude and phase. Among available phaseless techniques an iterative phaseless retrieval method [57] has been considered. Iterative techniques rely on the information provided by the spatial variation of the NF with distance and require the acquisition of the field on two or more surfaces [57], [58]. The main limitation is the risk of stagnation because of the use of iterative solvers for nonlinear systems of equations.

Because of mechanical restrictions in the measurement setup (Fig. 16), a radiated field can be acquired in the truncated spherical domains with  $0.5^\circ$  resolution in both the  $\theta$  and  $\varphi$  angles. The NF measurement results are depicted in Fig. 18 at 140 GHz, the highest frequency of the band

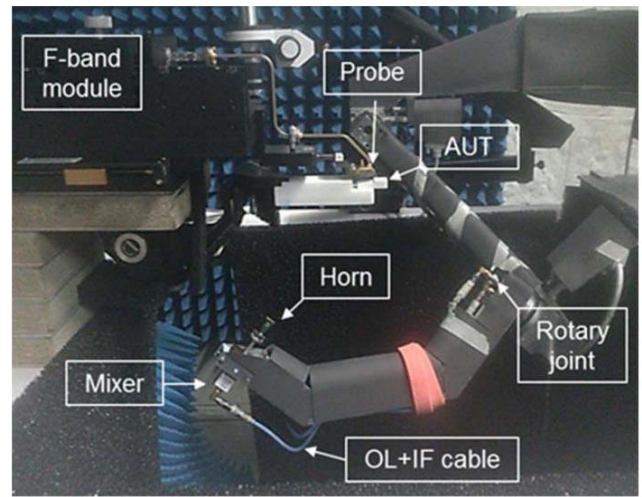
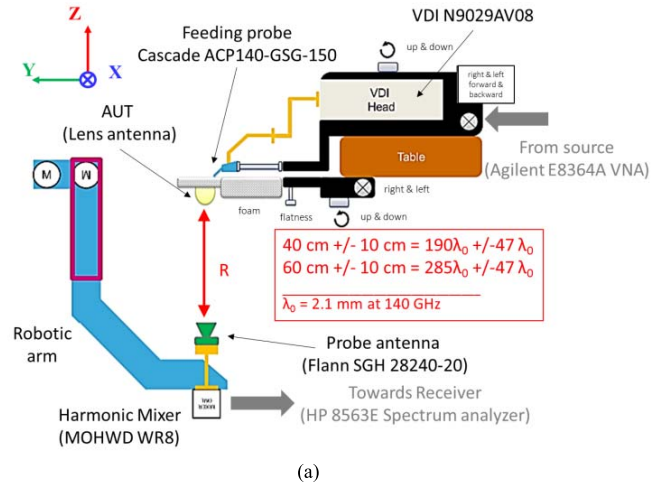


Fig. 16. (a) Scheme of the measurement setup. (b) Measurement setup arrangement and mounting.

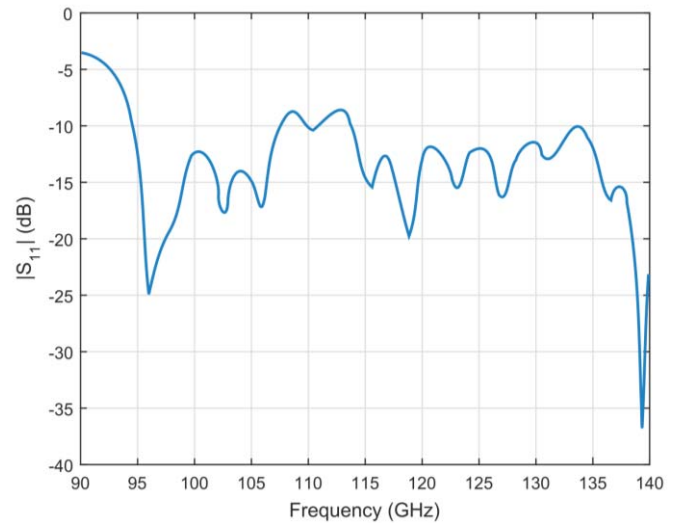


Fig. 17. Measured  $|S_{11}|$  of the full antenna system. BGA source radiating into the plastic support and the dome lens.

in which positioning and sampling errors can have a greater effect during the NF-FF transformation. Notice that the cross-polarization level is close to the average noise floor level,

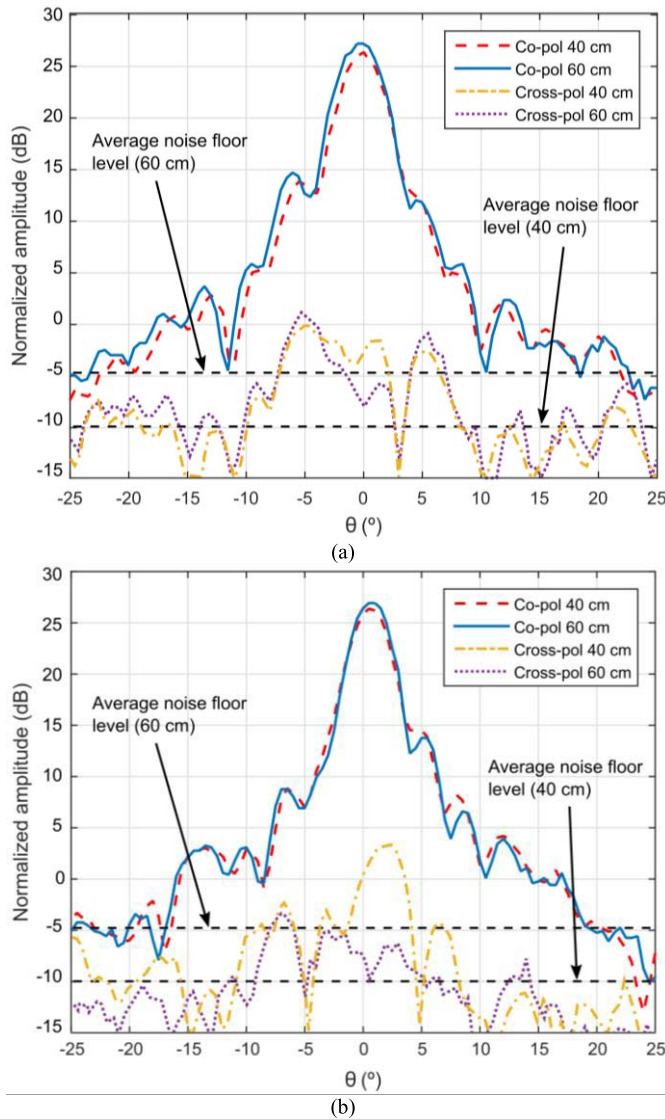


Fig. 18. NF measured at  $R = 40$  and  $60$  cm,  $f = 140$  GHz, for the main cuts. (a) H-plane ( $\varphi = 0^\circ$ ). (b) E-plane ( $\varphi = 90^\circ$ ).

so only the co-polar component at  $R = 40$  and  $60$  cm was considered for NF-FF transformation.

The phaseless NF-FF transformation is outlined in [57]. The goal of the technique was to compute a magnetic current distribution in the aperture from the NF amplitude acquired. Therefore, a cost function was set that related the amplitude of the measured field and the amplitude of the field radiated by the equivalent magnetic currents at both observation surfaces ( $R = 40$  and  $60$  cm). This cost function is nonlinear, so minimization techniques, such as Levenberg–Marquardt, that provide a monotonic decrease in the error were considered. The iterative solver stops when the error between the iterations  $n$  and  $n + 1$  is less than 0.001, or if the number of iterations is greater than 50. For this problem, the number of NF samples was 7062 (3531 samples per acquisition surface), and the number of unknowns was 841 (aperture plane of the Antenna Under Test discretization into  $29 \times 29$  subdomains). A Graphics Processing Unit implementation has been developed [57], so the calculation time is less than 10 s overall.

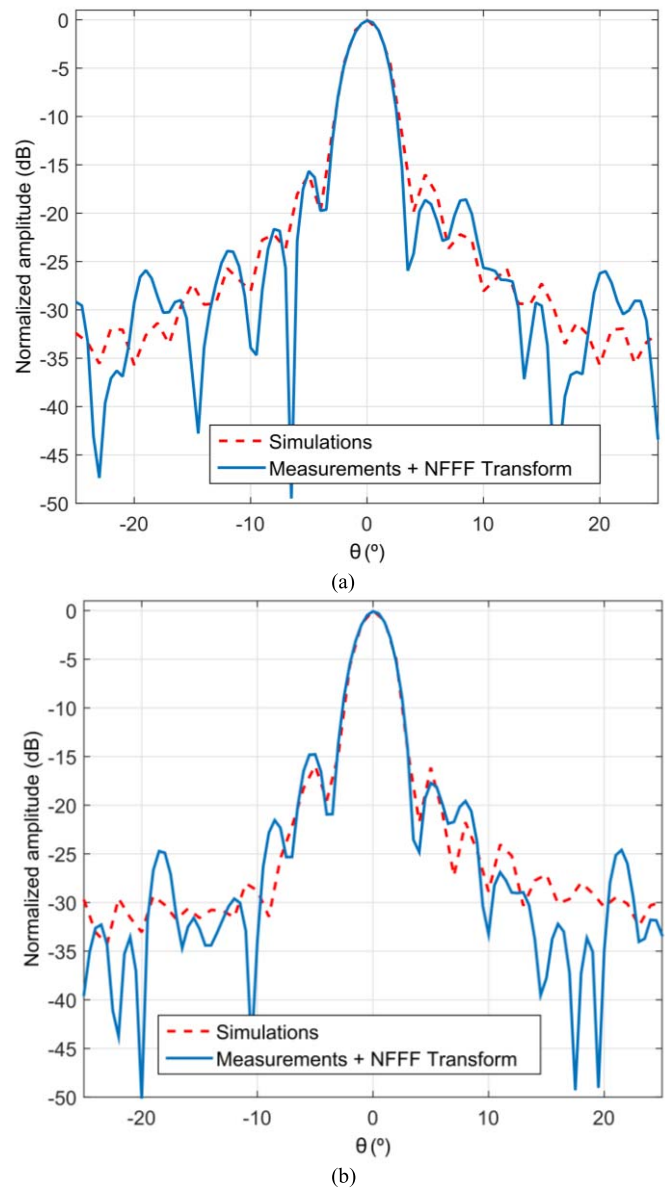


Fig. 19. Full antenna-system radiation patterns at  $f = 140$  GHz. Comparison between FF simulations and measurement results. (a) H-plane ( $\varphi = 0^\circ$ ). (b) E-plane ( $\varphi = 90^\circ$ ).

Next, the FF can be evaluated from the reconstructed equivalent magnetic currents on the lens antenna aperture. A comparison between the lens antenna patterns obtained from simulations and from NF measurements followed by a NF-FF transformation is plotted in Fig. 19 at 140 GHz. The agreement between the FF simulation and the NF-FF transformation obtained from the measurements was good for both planes of the main lobe and first sidelobes within the valid margin of the NF-FF transformation. The directivity was calculated by integrating the radiation pattern, which yielded 35.7 dB for simulation results, and  $D_{\text{lens,FF}} = 34.6$  dB in the case of NF measurements followed by a NF-FF transformation.

The lens antenna gain was obtained by means of the well-known intercomparison technique [59] with a standard gain horn in the  $F$ -band. As the lens antenna gain is measured in the NF region, NF-FF compensation must be applied

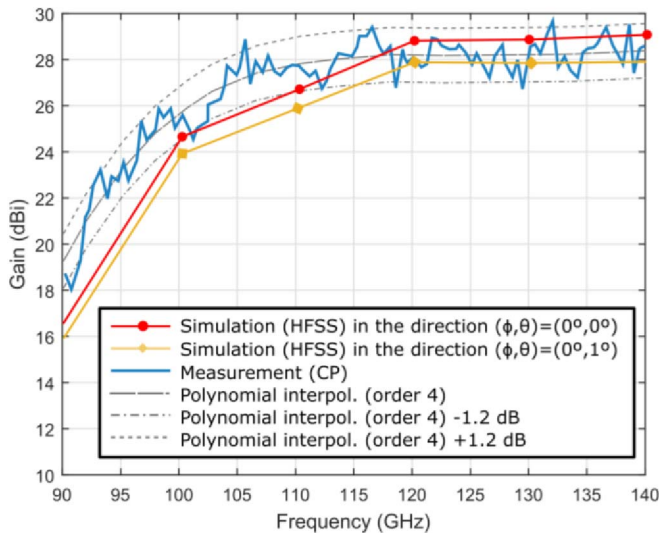


Fig. 20. Simulated (FF) and measured (NF  $\gg$  FF and gain compensation) dome lens antenna gain in the F-band. Measurements were fitted according to a fourth-order polynomial.

as follows:

$$G_{\text{lens,FF}}[\text{dBi}] = G_{\text{lens,NF}} + (D_{\text{lens,FF}} - D_{\text{lens,NF}}) \quad (5)$$

where  $G_{\text{lens,NF}} = 26.4$  dBi at 140 GHz (Fig. 18), and  $D_{\text{lens,FF}} = 34.6$  dBi.  $D_{\text{lens,NF}}$  was calculated by integrating the NF pattern at 60 cm, yielding  $D_{\text{lens,NF}} = 32.5$  dBi. Thus,  $G_{\text{lens,FF}} = 28.5$  dBi, just 0.5 dB lower than the value obtained from FF simulations (Fig. 20, simulation results: 29 dBi at 140 GHz). It also should be noted that simulated values of the gain with a  $1^\circ$  offset from the broadside direction were used in the computations, which were fully consistent with the offset observed in 40 and 60 cm NF radiation patterns in Fig. 18(b), primarily because of alignment inaccuracy.

Finally, the main cuts of the measured antenna patterns after NF-FF transformation are shown in Fig. 21 for three different frequencies. Low variability in the radiation pattern versus frequency was observed in the FF.

#### IV. ACTIVE MEASUREMENTS FOR 5G BACKHAUL/FRONTHAUL LINKS

For 5G point-to-point backhaul links, the full antenna system was integrated with a specially designed transceiver chip [60] (Fig. 22).

An effective isotropic radiated power (EIRP) of more than 33 dBm was measured for the Tx with the lens. Data rates above 12 Gbps with less than  $10^{-6}$  bit error rate (BER) were achieved at nearly 5 m in a complex nonideal scenario with a metal reflector that closes the Tx-Rx loop. The energy efficiency achieved was better than 1.6 pJ/b/m, at least 40 times better than state-of-the-art high-speed transceivers [13], [61]–[67] because of the high EIRP/ $P_{\text{DC,TX}}$  ( $>130$  times compared to [61]–[66]) achieved with the high gain compact antenna system and the use of energy-efficient OOK modulation schemes, yielding a low-cost and low-consumption system.

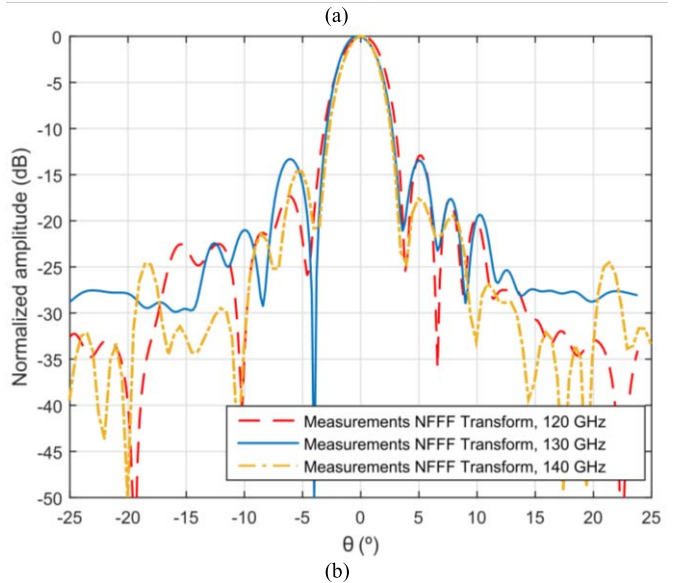
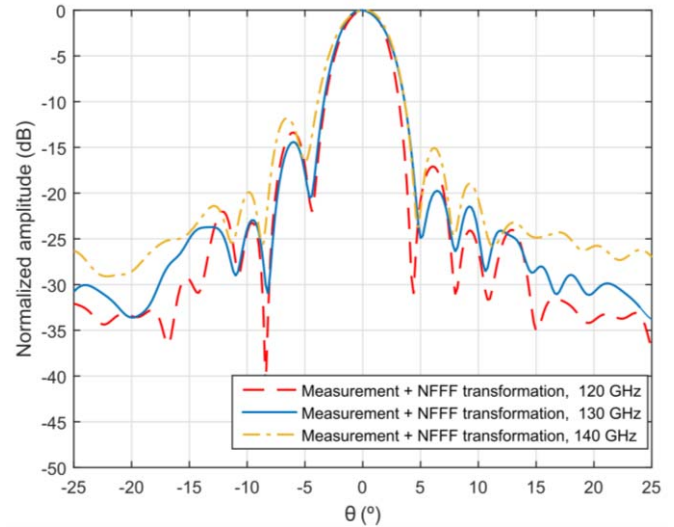


Fig. 21. FF pattern comparison at different frequencies. (a) H-plane ( $\phi = 0^\circ$ ). (b) E-plane ( $\phi = 90^\circ$ ).



Fig. 22. Fully packaged system with active chip and lens integrated on the PC board for 5G backhaul links.

#### V. CONCLUSION

This paper proposed a BGA module with an integrated 3-D-printed plastic lens for application in a dedicated 130 GHz

OOK transceiver that targets 5G backhaul/fronthaul systems. First, the BGA module technology and the design of an efficient planar source antenna were described. The source antenna was a  $2 \times 2$  array of aperture-coupled patch antennas integrated in the BGA module of  $7 \times 7 \times 0.362 \text{ mm}^3$ . It exhibited more than 7.8 dBi realized gain, broadside polarization purity greater than 20 dB, and over 55% total efficiency from 110 to 140 GHz (20% bandwidth). Second, the design, fabrication, and measurement of the ABS-plastic lens using the BGA module as a source feed were presented. Measurement results largely were consistent with simulations in particular, greater than 28 dBi realized gain from 114 to 140 GHz (20% bandwidth) was achieved. Finally, active measurements together with a transceiver demonstrated data rates higher than 12 Gbps with a BER less than  $10^{-6}$  at nearly 5 m, showing the potential for the antenna system proposed in this paper. These results are promising, and the performance achieved represents a contribution to cost-effective, energy-efficient backhaul/fronthaul systems for 5G. Future research will focus on the design of competitive prototypes with more efficient sources with radiation pattern stability and higher total efficiency.

#### REFERENCES

- [1] Y. Niu, Y. Li, D. Jin, L. Su, and A. V. Vasilakos, "A survey of millimeter wave communications (mmWave) for 5G: Opportunities and challenges," *Wireless Netw.*, vol. 21, no. 8, pp. 2657–2676, Nov. 2015.
- [2] "5G candidate band study. Study on the suitability of potential candidate frequency bands above 6 GHz for future 5G mobile broadband systems," Ofcom, London, U.K., Final Rep., Mar. 2015. [Online]. Available: <http://www.QuotientAssociates.com>
- [3] J. Wells, "Faster than fiber: The future of multi-G/s wireless," *IEEE Microw. Mag.*, vol. 10, no. 3, pp. 104–112, May 2009.
- [4] *Microwave Towards 2020: Delivering High-Capacity and Cost-Efficient Backhaul for Broadband Networks Today and in the Future*, Ericsson, Stockholm, Sweden, Sep. 2015
- [5] M. Pagani, "The trends and challenges of microwave/millimeter-wave in future 5G wireless communication networks," in *IEEE Proc. Int. Microw. Symp., Workshop WME, Front-End Module (FEM) 5G*, Honolulu, HI, USA, Jun. 2017.
- [6] European Commission. *RSPG Report on Spectrum Issues on Wireless Backhaul, Radio Spectrum Policy Group*. Accessed: Jan. 2, 2017. [Online]. Available: [http://rspg-spectrum.eu/wp-content/uploads/2013/05/RSPG15-607-Final\\_Report-Wireless\\_backhaul.pdf](http://rspg-spectrum.eu/wp-content/uploads/2013/05/RSPG15-607-Final_Report-Wireless_backhaul.pdf)
- [7] L. Verma, M. Fakhrazadeh, and S. Choi, "Backhaul need for speed: 60 GHz is the solution," *IEEE Wireless Commun.*, vol. 22, no. 6, pp. 114–121, Dec. 2015.
- [8] T. S. Rappaport, J. N. Murdock, and F. Gutierrez, Jr., "State of the art in 60-GHz integrated circuits and systems for wireless communications," *Proc. IEEE*, vol. 99, no. 8, pp. 1390–1436, Aug. 2011.
- [9] B. Ayzavian, "Second generation E-band solutions: Opportunities for carrier-class LTE backhaul," Heavy Reading, White paper, Accessed: Jan. 2, 2017. [Online]. Available at: <http://www.huawei.com/au/static/HW-206551.pdf>
- [10] E. Johnson, "Mobile data backhaul: The need for E-band," *Mobile World Congr.*, 2013, Accessed: Jan. 2, 2017. [Online]. Available: <http://www.microwavejournal.com/ext/resources/whitepapers/2013/february/Sky-Light-Research-E-Band.pdf?1471624980>
- [11] (Oct. 11, 2016). *E-Band Millimeter Wave Technology*, Microwave Link. Accessed: Jan. 2, 2017. [Online]. Available at: <http://www.microwave-link.com/microwave/e-band-millimeter-wave-technology/>
- [12] B. Panzner, "Scheduling conflicts in wireless in-band backhaul for 5G millimeter wave communications," in *Proc. IEEE Conf. Comput. Commun. Workshops (INFOCOM WKSHPS)*, San Francisco, CA, USA, Apr. 2016, pp. 110–111.
- [13] N. Deferm and P. Reynaert, "A 120 GHz fully integrated 10 Gb/s short-range star-QAM wireless transmitter with on-chip bondwire antenna in 45 nm low power CMOS," *IEEE J. Solid-State Circuits*, vol. 49, no. 7, pp. 1606–1616, Jul. 2014.
- [14] C. Wang, C. Lin, Q. Chen, B. Lu, X. Deng, and J. Zhang, "A 10-Gbit/s wireless communication link using 16-QAM modulation in 140-GHz band," *IEEE Trans. Microw. Theory Techn.*, vol. 61, no. 7, pp. 2737–2746, Jul. 2013.
- [15] I. Ando, M. Tanio, M. Ito, T. Kuwabara, T. Marumoto, and K. Kunihiro, "Wireless D-band communication up to 60 Gbits/s with 64QAM using GaAs HEMT technology," in *Proc. IEEE Radio Wireless Symp. (RWS)*, Austin, TX, USA, Jan. 2016, pp. 193–195.
- [16] H. Shams, M. J. Fice, L. Gonzalez-Guerrero, C. C. Renaud, F. van Dijk, and A. J. Seeds, "Sub-THz wireless over fiber for frequency band 220–280 GHz," *J. Lightw. Technol.*, vol. 34, no. 20, pp. 4786–4793, Oct. 15, 2016.
- [17] N. Sarmah, P. R. Vazquez, J. Grzyb, W. Foerster, B. Heinemann, and U. R. Pfeiffer, "A wideband fully integrated SiGe chipset for high data rate communication at 240 GHz," in *Proc. EuMA*, London, U.K., Oct. 2016, pp. 181–184.
- [18] D. Cohen, "5G and the IoT: 5 Trends and implications," *Microw. J.*, vol. 59, no. 9, pp. 44–48, Sep. 2016, Accessed: Jan. 2, 2017. [Online]. Available: <http://www.microwavejournal.com/articles/27058-g-and-the-iot-5-trends-and-implications>
- [19] A. Bisognin *et al.*, "Millimeter-wave antenna-in-package solutions for WiGig and backhaul applications," in *Proc. Int. Workshop Antenna Technol. (iWAT)*, Seoul, South Korea, Mar. 2015, pp. 52–55.
- [20] J. Chen *et al.*, "A digitally modulated mm-Wave Cartesian beamforming transmitter with quadrature spatial combining," in *IEEE Int. Solid-State Circuits Conf. (ISSCC) Dig. Tech. Papers*, San Francisco, CA, USA, Feb. 2013, pp. 232–233.
- [21] A. Townley *et al.*, "A 94GHz 4TX-4RX phased-array for FMCW radar with integrated LO and flip-chip antenna package," in *Proc. Radio Freq. Integr. Circuits Symp. (RFIC)*, San Francisco, CA, USA, Jun. 2016.
- [22] K. Lee *et al.*, "Technology advancement of laminate substrates for mobile, IoT, and automotive applications," in *Proc. China Semiconductor Technol. Int. Conf. (CSTIC)*, Mar. 2017, pp. 1–4.
- [23] B. M. D. Sawyer *et al.*, "Design and demonstration of a 2.5-D glass interposer BGA package for high bandwidth and low cost," *IEEE Trans. Compon., Packag., Manuf. Technol.*, vol. 7, no. 4, pp. 552–562, Apr. 2017.
- [24] R. Pilard *et al.*, "HDI organic technology integrating built-in antennas dedicated to 60 GHz SiP solution," in *Proc. IEEE Int. Symp. Antennas Propag. (APS)*, Chicago, IL, USA, Jul. 2012, pp. 1–2.
- [25] S. Beer *et al.*, "An integrated 122-GHz antenna array with wire bond compensation for SMT radar sensors," *IEEE Trans. Antennas Propag.*, vol. 61, no. 12, pp. 5976–5983, Dec. 2013.
- [26] D. Liu and Y. P. Zhang, "Integration of array antennas in chip package for 60-GHz radios," *Proc. IEEE*, vol. 100, no. 7, pp. 2364–2371, Jul. 2012.
- [27] A. Valdes-Garcia *et al.*, "A fully integrated 16-element phased-array transmitter in SiGe BiCMOS for 60-GHz communications," *IEEE J. Solid-State Circuits*, vol. 45, no. 12, pp. 2757–2773, Dec. 2010.
- [28] D. G. Kam, D. Liu, A. Natarajan, S. K. Reynolds, and B. A. Floyd, "Organic packages with embedded phased-array antennas for 60-GHz wireless chipsets," *IEEE Trans. Compon., Packag., Manuf. Technol.*, vol. 1, no. 11, pp. 1806–1814, Nov. 2011.
- [29] S. Brebels, A. Enayati, C. Soens, W. De Raedt, L. Van der Perre, and G. A. E. Vandenbosch, "Technologies for integrated mm-Wave antennas," in *Proc. 8th Eur. Conf. Antennas Propag. (EuCAP)*, Apr. 2014, pp. 727–731.
- [30] S. Zahir, O. D. Gurbuz, A. Kar-Roy, S. Raman, and G. M. Rebeiz, "60-GHz 64- and 256-elements wafer-scale phased-array transmitters using full-reticle and subreticle stitching techniques," *IEEE Trans. Microw. Theory Techn.*, vol. 64, no. 12, pp. 4701–4719, Dec. 2016.
- [31] W. Zhang, Y. P. Zhang, M. Sun, C. Luxey, D. Titz, and F. Ferrero, "A 60-GHz circularly-polarized array antenna-in-package in LTCC technology," *IEEE Trans. Antennas Propag.*, vol. 61, no. 12, pp. 6228–6232, Dec. 2013.
- [32] B. Zhang, Y. P. Zhang, D. Titz, F. Ferrero, and C. Luxey, "A circularly-polarized array antenna using linearly-polarized sub grid arrays for highly-integrated 60-GHz radio," *IEEE Trans. Antennas Propag.*, vol. 61, no. 1, pp. 436–439, Jan. 2013.
- [33] Z. Chen, Y. P. Zhang, A. Bisognin, D. Titz, F. Ferrero, and C. Luxey, "An LTCC microstrip grid array antenna for 94-GHz applications," *IEEE Antennas Wireless Propag. Lett.*, vol. 14, pp. 1279–1281, 2015.
- [34] X. Gu, A. Valdes-Garcia, A. Natarajan, B. Sadhu, D. Liu, and S. K. Reynolds, "W-band scalable phased arrays for imaging and communications," *IEEE Commun. Mag.*, vol. 53, no. 4, pp. 196–204, Apr. 2015.

- [35] S. Brebels *et al.*, “60-GHz CMOS TX/RX chipset on organic packages with integrated phased-array antennas,” in *Proc. 10th Eur. Conf. Antennas Propag. (EuCAP)*, Apr. 2016, pp. 1–5.
- [36] G. Mangraviti *et al.*, “A 4-antenna-path beamforming transceiver for 60 GHz multi-Gb/s communication in 28 nm CMOS,” in *IEEE Int. Solid-State Circuits Conf. (ISSCC) Dig. Tech. Papers*, San Francisco, CA, USA, Jan./Feb. 2016, pp. 246–247.
- [37] A. Townley *et al.*, “A 94-GHz 4TX–4RX phased-array FMCW radar transceiver with antenna-in-packag,” *IEEE J. Solid-State Circuits*, vol. 52, no. 5, pp. 1245–1259, May 2017.
- [38] A. Tomkins *et al.*, “A 60 GHz, 802.11ad/WiGig-compliant transceiver for infrastructure and mobile applications in 130 nm SiGe BiCMOS,” *IEEE J. Solid-State Circuits*, vol. 50, no. 10, pp. 2239–2255, Oct. 2015.
- [39] C. Beck *et al.*, “Industrial mmWave radar sensor in embedded wafer-level BGA packaging technology,” *IEEE Sensors J.*, vol. 16, no. 17, pp. 6566–6578, Sep. 2016.
- [40] Y. Tsutsumi, T. Ito, K. Hashimoto, S. Obayashi, H. Shoki, and H. Kasami, “Bonding wire loop antenna in standard ball grid array package for 60-GHz short-range wireless communication,” *IEEE Trans. Antennas Propag.*, vol. 61, no. 4, pp. 1557–1563, Apr. 2013.
- [41] S. Li, T. Chi, J. S. Park, W. T. Khan, H. Wang, and J. Papapolymerou, “A fully packaged D-band MIMO transmitter using high-density flip-chip interconnects on LCP substrate,” in *IEEE MTT-S Int. Microw. Symp. Dig.*, May 2016, pp. 1–4.
- [42] T. Braun *et al.*, “Opportunities of fan-out wafer level packaging (FOWLP) for RF applications,” in *Proc. IEEE 16th Top. Meet. Silicon Monolithic Integr. Circuits RF Syst. (SiRF)*, Jan. 2016, pp. 35–37.
- [43] B. P. Ginsburg, S. M. Ramaswamy, V. Rentala, E. Seok, S. Sankaran, and B. Haroun, “A 160 GHz pulsed radar transceiver in 65 nm CMOS,” *IEEE J. Solid-State Circuits*, vol. 49, no. 4, pp. 984–995, Apr. 2014.
- [44] D. Titz, F. Ferrero, and C. Luxey, “Development of a millimeter-wave measurement setup and dedicated techniques to characterize the matching and radiation performance of probe-fed antennas,” *IEEE Antennas Propag. Mag.*, vol. 54, no. 4, pp. 188–203, Aug. 2012.
- [45] A. Bisognin *et al.*, “Probe-fed measurement system for F-band antennas,” in *Proc. Eur. Conf. Antennas Propag. (EuCAP)*, The Hague, The Netherlands, Apr. 2014, pp. 722–726.
- [46] D. Titz, F. Ferrero, P. Brachet, C. Luxey, and G. Jacquemod, “Efficiency measurement of probe-fed antennas operating at millimeter-wave frequencies,” *IEEE Antennas Wireless Propag. Lett.*, vol. 11, pp. 1194–1197, 2012.
- [47] J. M. Edwards and G. M. Rebeiz, “High-efficiency silicon RFIC millimeter-wave elliptical slot-antenna with a quartz lens,” in *Proc. IEEE Int. Symp. Antennas Propag. (APSURSI)*, Spokane, WA, USA, Jul. 2011, pp. 899–902.
- [48] A. Artemenko, A. Mozharovskiy, A. Maltsev, R. Maslennikov, A. Sevastyanov, and V. Ssorin, “Experimental characterization of E-band two-dimensional electronically beam-steerable integrated lens antennas,” *IEEE Antennas Wireless Propag. Lett.*, vol. 12, pp. 1188–1191, 2013.
- [49] H. Gulan, C. Rusch, S. Beer, T. Zwick, M. Kuri, and A. Tessmann, “Lens coupled broadband slot antenna for W-band imaging applications,” in *Proc. IEEE Antennas Propag. Soc. Int. Symp. (APSURSI)*, Orlando, FL, USA, Jul. 2013, pp. 424–425.
- [50] H. Yi, S.-W. Qu, K.-B. Ng, C. H. Chan, and X. Bai, “3-D printed millimeter-wave and Terahertz lenses with fixed and frequency scanned beam,” *IEEE Trans. Antennas Propag.*, vol. 64, no. 2, pp. 442–449, Feb. 2016.
- [51] R. Gonçalves, N. B. Carvalho, and P. Pinho, “Wireless energy transfer: Dielectric lens antennas for beam shaping in wireless power-transfer applications,” *Comp. Rendus Phys.*, vol. 18, no. 2, pp. 78–89, Feb. 2017. [Online]. Available: <http://dx.doi.org/10.1016/j.crhy.2016.11.004>
- [52] M. G. Silveirinha, C. A. Fernandes, and J. R. Costa, “A graphical aid for the complex permittivity measurement at microwave and millimeter wavelengths,” *IEEE Microw. Wireless Compon. Lett.*, vol. 24, no. 6, pp. 234–241, Jun. 2014.
- [53] E. Saenz, L. Rolo, K. van't Klooster, M. Paquay, and V. V. Parshin, “Accuracy assesment of material measurements with a quasi-optical free-space test bench,” in *Proc. Eur. Conf. Antennas Propag. (EuCAP)*, Prague, Czech Republic, Mar. 2012, pp. 149–152.
- [54] D. F. Filipovic, S. S. Gearhart, and G. M. Rebeiz, “Double-slot antennas on extended hemispherical and elliptical silicon dielectric lenses,” *IEEE Trans. Microw. Theory Techn.*, vol. 41, no. 10, pp. 1738–1749, Oct. 1993.
- [55] C. A. Fernandes, J. R. Costa, and E. B. Lima, “Dielectric lens antennas,” in *Handbook of Antenna Technologies*, Z. N. Chen, D. Liu, H. Nakano, X. Qing, and T. Zwick, Eds. Singapore: Springer, 2016.
- [56] E. Lima, J. R. Costa, M. G. Silveirinha, and C. A. Fernandes, “ILASH—Software tool for the design of integrated lens antennas,” in *Proc. IEEE Antennas Propag. Soc. Int. Symp. (AP-S Symp)*, New York, NY, USA, Jul. 2008, pp. 1–4.
- [57] Y. Álvarez, F. Las-Heras, and M. R. Pino, “The sources reconstruction method for amplitude-only field measurements,” *IEEE Trans. Antennas Propag.*, vol. 58, no. 8, pp. 2776–2781, Aug. 2010.
- [58] S. F. Razavi and Y. Rahmat-Samii, “Phaseless measurements over non-rectangular planar near-field systems without probe corotation,” *IEEE Trans. Antennas Propag.*, vol. 61, no. 1, pp. 143–152, Jan. 2013.
- [59] *IEEE Standard Test Procedures for Antennas*, ANSI/IEEE Standard 149-1979, New York, NY, USA, 1979.
- [60] N. Dolatsha *et al.*, “A compact 130 GHz fully packaged point-to-point wireless system with 3D-printed 26 dBi lens antenna achieving 12.5 Gb/s at 1.55 pJ/bm,” in *IEEE Int. Solid-State Circuits Conf. (ISSCC) Dig. Tech. Papers*, San Francisco, CA, USA, Feb. 2017, pp. 306–307.
- [61] C. W. Byeon, C. H. Yoon, and C. S. Park, “A 67-mW 10.7-Gb/s 60-GHz OOK CMOS transceiver for short-range wireless communications,” *IEEE Trans. Microw. Theory Techn.*, vol. 61, no. 9, pp. 3391–3401, Sep. 2013.
- [62] Z. Wang, P.-Y. Chiang, P. Nazari, C.-C. Wang, Z. Chen, and P. Heydari, “A CMOS 210-GHz fundamental transceiver with OOK modulation,” *IEEE J. Solid-State Circuits*, vol. 49, no. 3, pp. 564–580, Mar. 2014.
- [63] S. Shahramian, M. J. Holyoak, and Y. Baeyens, “A 16-element W-band phased array transceiver chipset with flip-chip PCB integrated antennas for multi-gigabit data links,” in *Proc. IEEE Radio Freq. Integr. Circuits Symp.*, May 2015, pp. 27–30.
- [64] S. V. Thyagarajan, S. Kang, and A. M. Niknejad, “A 240 GHz fully integrated wideband QPSK receiver in 65 nm CMOS,” *IEEE J. Solid-State Circuits*, vol. 50, no. 10, pp. 2268–2280, Oct. 2015.
- [65] R. Wu *et al.*, “A 42 Gb/s 60 GHz CMOS transceiver for IEEE 802.11ay,” in *IEEE ISSCC Dig. Tech. Papers*, Jan./Feb. 2016, pp. 248–249.
- [66] K. K. Tokgoz *et al.*, “A 56 Gb/s W-band CMOS wireless transceiver,” in *IEEE ISSCC Dig. Tech. Papers*, Jan./Feb. 2016, pp. 242–243.
- [67] M. Pierpoint and G. M. Rebeiz, “Paving the way for 5G realization and mmWave communication systems,” *Microw. J.*, vol. 59, no. 4, pp. 1–3, Apr. 2016, Accessed: Jan. 2, 2017. [Online]. Available: <http://www.microwavejournal.com/articles/26255-paving-the-way-for-5g-realization-and-mmwave-communication-systems?v=preview>



**Aimeric Bisognin** (S'13) was born in Toulouse, France, in 1989. He received the engineering degree in electronics from Polytech'Nice Sophia, Biot, France, in 2012, the M.S. degree in telecommunications from EDSTIC, Sophia Antipolis, France, in 2012, and the Ph.D. (Hons.) degree in electronics engineering from the University of Nice Sophia-Antipolis, Nice, France, in 2015.

During his Ph.D., he was with the Electronique pour Objets Communicants (EPOC) Laboratory, STMicroelectronics, Crolles, France. He is currently a Post-Doctoral Researcher with the EPOC Laboratory. He has authored or co-authored eight publications in journals and 19 publications in international conferences. His current research interests include millimeter-wave communications, especially in the field of the design and measurement of antenna in package, lens and reflector antennas for the 60, 80, and 120 GHz frequency bands.



**Nour Nachabe** was born in Tripoli, Lebanon, in 1992. She received the bachelor's degree in electrical and electronics engineering and the master's degree in telecommunications from the Lebanese University, Tripoli, in 2015. She has been pursuing the Ph.D. degree with Université Côte d'Azur, Nice, France, since 2015.

She has been with Polytech'Lab, Université Côte d'Azur, since 2015. Her current research interests include design and measurement of millimeter-wave antennas, wide band array antennas, and additive manufacturing technologies for building RF components in millimeter-wave frequency bands.



**Cyril Luxey** (M'05–SM'09–F'17) was born in Nice, France, in 1971. He received the Ph.D. degree in electrical engineering from the University Nice-Sophia Antipolis, Nice, France, in 1999. His dissertation focused on several antenna concepts for automotive applications such as printed leaky-wave antennas, quasi-optical mixers and retrodirective transponders.

From 2000 to 2002, he was with Alcatel, Mobile Phone Division, Colombes, France, where he was involved in the design and integration of internal antennas for commercial mobile phones. He was a Junior Member of the Institut Universitaire de France (IUF) institution for five years. He was an Associate Professor with the Polytechnic School, University Nice Sophia-Antipolis, in 2003. Since 2009, he has been a Full Professor with the IUT Réseaux et Télécoms, Sophia-Antipolis, France, where he is doing research in Polytech'Lab. He has authored or co-authored more than 300 papers in refereed journals, in international and national conferences, and in book chapters. His current research interests include the design and measurement of millimeter-wave antennas, antennas-in-package, plastic lenses, organic modules for mm-wave and sub-millimeter-wave frequency bands, electrically small antennas, multiantenna systems for diversity, and MIMO techniques.

Dr. Luxey was the General Chair of the Loughborough Antennas and Propagation Conference 2011, the award and Grant Chair of EuCAP 2012, and the invited paper Co-Chair of EuCAP 2013. He is the TPC chair of EuCAP 2017 conference in Paris. He has given more than 15 invited talks. Since 2015, he has been a member of the IEEE AP-S Education committee. He was an Associate Editor of the IEEE ANTENNAS AND WIRELESS PROPAGATION LETTERS from 2012 to 2017, a reviewer for the IEEE TRANSACTIONS ON ANTENNAS AND PROPAGATION, the IEEE ANTENNAS AND WIRELESS PROPAGATION LETTERS, the IEEE TRANSACTIONS ON MICROWAVE THEORY AND TECHNIQUES, the IEEE MICROWAVE AND WIRELESS CONFERENCE LETTERS, the *IET Electronics Letters*, the *IET Microwave Antennas and Propagation* journals and several European and U.S. conferences in the field of microwave, microelectronics, and antennas. He and his students received the H.W. Wheeler Award of the IEEE Antennas and Propagation Society for the best application paper of the year 2006. He is also a co-recipient of the Jack Kilby Award 2013 of the ISSCC conference. He was a co-recipient of the best paper of the EUCAP2007 conference, the best-paper award of the International Workshop on Antenna Technology (iWAT2009), the best paper award at LACP 2012, the best student paper at LACP 2013 (third place), the best paper of the ICEAA 2014 conference, and the best paper of the innovation contest of the iWEM 2014 conference (second place). He was a recipient of the University Nice-Sophia Antipolis Medal in 2014 and the University Côte d'Azur medal in 2016.



**Frédéric Giancesello** (M'13) received the B.S. and M.S. degrees in electronics engineering from the Institut National Polytechnique de Grenoble, Grenoble, France, in 2003, and the Ph.D. degree in electrical engineering from the Joseph Fourier University, Grenoble, in 2006.

He is currently with STMicroelectronics, Crolles, France, where he leads the team responsible for the development of electromagnetic devices (inductor, balun, transmission line, and antenna) integrated on advanced RF CMOS/BiMOS (down to 14 nm), silicon photonics, and advanced packaging technologies (3-D Integration, FOWLP, etc.). He has authored and co-authored more than 110 refereed journal and conference technical articles.

Dr. Giancesello has served on the TPC for the International SOI Conference from 2009 to 2011 and he is currently serving on the TPC for the Loughborough Antennas and Propagation Conference.



**Daniel Gloria** received the engineering degree in electronics from the Ecole Nationale Supérieure d'Electronique et de Radioélectrique, Grenoble, France, in 1995, and the M.S.E.E. degree in optics, optoelectronics, and microwave design systems from the Institut National de Grenoble, Grenoble.

He was an RF Designer Engineer with ALCATEL Bell Network System Labs, Charleroi, Belgium, from 1995 to 1997, where he was involved in the development of the Cablephone RF front end and its integration in hybrid-fiber-coax telecommunication networks. Since 1997, he has been with TPS Laboratory, ST Microelectronics, Technology Research and Development, Crolles, France, where he is in charge of HF Characterization and RF Passive Modeling Group. His current research interests include optimization of active and passive devices for HF applications in BiCMOS and CMOS advanced technologies.



**Jorge R. Costa** (S'97–M'03–SM'09) was born in Lisbon, Portugal, in 1974. He received the Licenciado and Ph.D. degrees in electrical and computer engineering from the Instituto Superior Técnico, Technical University of Lisbon, Lisbon, Portugal, in 1997 and 2002, respectively.

He is currently a Researcher with the Instituto de Telecomunicações, Lisbon, Portugal. He is also an Associate Professor with the Departamento de Ciências e Tecnologias da Informação, Instituto Universitário de Lisboa, Lisbon. He has authored or co-authored more than 150 papers in peer reviewed journals and international conference proceedings. More than 30 of these papers have appeared in IEEE Journals. He has co-authored four patent applications. His current research interests include lenses, reconfigurable antennas, MEMS switches, UWB, and MIMO and RFID antennas.

Prof. Costa was an Associate Editor of the IEEE TRANSACTIONS ON ANTENNAS AND PROPAGATION from 2010 to 2016, and was a Guest Editor of the Special Issue on "Antennas and Propagation at mm- and Sub-mm Waves," in the IEEE TRANSACTIONS ON ANTENNAS AND PROPAGATION, in 2013. He was the Co-Chair of the Technical Program Committee of the European Conference on Antennas and Propagation (EuCAP 2015) in Lisbon and General Vice-Chair of EuCAP 2017 in Paris.



**Carlos A. Fernandes** (S'86–M'89–SM'08) received the Licenciado, M.Sc., and Ph.D. degrees in electrical and computer engineering from Instituto Superior Técnico (IST), Technical University of Lisbon, Lisbon, Portugal, in 1980, 1985, and 1990, respectively.

He joined IST in 1980, where he is currently a Full Professor with the Department of Electrical and Computer Engineering, where he is involved in microwaves, radio wave propagation, and antennas. He is a Senior Researcher with the Instituto de

Telecomunicações and member of the Board of Directors. He has authored or co-authored a book, two book chapters, more than 180 technical papers in peer-reviewed international journals and conference proceedings, and seven patents in the areas of antennas and radiowave propagation modeling. His current research interests include dielectric antennas for millimeter wave applications, antennas and propagation modeling for personal communication systems, RFID and UWB antennas, artificial dielectrics and metamaterials.

Dr. Fernandes was a Guest Editor of the Special Issue on "Antennas and Propagation at mm- and sub-mm waves," in the IEEE TRANSACTIONS ON ANTENNAS AND PROPAGATION, in 2013.



**Yuri Alvarez** (S'06–M'09–SM'15) was born in Langreo, Spain, in 1983. He received the M.S. and Ph.D. degrees in telecommunication engineering from the University of Oviedo, Gijón, Spain, in 2006 and 2009, respectively.

He was a Visiting Scholar with the Department of Electrical Engineering and Computer Science, Syracuse University, Syracuse, NY, USA, in 2006 and 2008; a Visiting Post-Doctoral Researcher at the Gordon Center for Subsurface Sensing and Imaging Systems (CenSSIS) ALERT

(Awareness and Localization of Explosive Related Threats) Center of Excellence, Northeastern University, Boston, MA, USA, from 2011 to 2014; and a Visiting Post-Doctoral Researcher at ELEDIA Research Center, Trento, Italy, in 2015. He is currently an Assistant Professor with the Signal Theory and Communications, University of Oviedo, Gijón, Spain. His current research interests include antenna diagnostics, antenna measurement techniques, RF techniques for indoor location, inverse scattering and imaging techniques, and phaseless methods for antenna diagnostics and imaging.

Dr. Alvarez was a recipient of the 2011 Regional and National Awards to the Best Ph.D. Thesis on Telecommunication Engineering (category: security and defense).



**Ana Arboleya-Arboleya** received the M.Sc. degree in telecommunication engineering and the Ph.D. degree in telecommunication engineering from the University of Oviedo, Oviedo, Spain, in 2009 and 2016, respectively.

From 2008 to 2016, she was a Research Assistant with the Signal Theory and Communications Research Group, TSC-UNIOVI, Department of Electrical Engineering, University of Oviedo. She was a Visiting Scholar with MilliLab, Department of Radio Science and Engineering, Aalto University, Espoo, Finland, from 2014 to 2015. She is currently a Post-Doctoral Researcher with the EpOC Polytech' Lab (Electronics for Connected Objects), the University of Nice Sophia-Antipolis, Nice, France. Her current research interests include antenna diagnostics, measurement systems and techniques, and high-frequency imaging techniques and applications.

Dr. Arboleya was a recipient of the 2017 National Awards of the Official College of Telecommunication Engineers of Spain to the Best Ph.D. Thesis on telecommunication engineering in the category of security and defense.



**Jaime Laviada** was born in Gijón, Spain. He received the M.S. degree in telecommunication engineering and the Ph.D. degree from the Universidad de Oviedo, Oviedo, Spain, in 2005 and 2010, respectively.

In 2006, he joined the Signal Theory and Communications Research Group, Universidad de Oviedo, where he was involved in multiple national and European projects as well as contracts with several companies. In 2015, he was with the Antennas Group, Universidad Pública de Navarra, Pamplona,

Spain, where he was collaborating in several applied research projects. He is currently an Assistant Professor with the Universidad de Oviedo. He was a Visiting Scholar with the Electromagnetics and Communications Lab, Pennsylvania State University, State College, PA, USA, from 2007 to 2008, as well as in the Applied Microwave Nondestructive Testing Laboratory, Missouri S&T, Rolla, MA, USA, in 2017.



**Fernando Las-Heras** (M'86–SM'08) received the M.S. degree in telecommunication engineering and the Ph.D. degree in telecommunication engineering from the Technical University of Madrid (UPM), Madrid, Spain, in 1987 and 1990, respectively.

He was a National Graduate Research Fellow from 1988 to 1990, and then an Associate Professor with the Department of Signal, Systems and Radiocommunications, UPM, from 1991 to 2000. He was a Visiting Lecturer with the National University of Engineering, Lima, Peru, in 1996; a Visiting

Researcher with Syracuse University, Syracuse, NY, USA, in 2000; and a short term Visiting Lecturer with ESIGELEC, Saint-Étienne-du-Rouvray, France, from 2005 to 2011. Since 2001, he heads the Research Group of Signal Theory and Communications TSC-UNIOVI, Department of Electrical Engineering, University of Oviedo, Oviedo, Spain. Since 2003, he has been a Full Professor with the University of Oviedo, where he was the Vice-Dean for Telecommunication Engineering, Technical School of Engineering, Gijón, Spain, from 2004 to 2008. He has authored over 300 articles in academic journals and proceedings of international conferences, mainly in the areas of antenna design and the inverse electromagnetic problem with applications in diagnostic, measurement and synthesis of antennas, metasurfaces, phaseless techniques, propagation, and microwave to THz imaging and localization, as well as in engineering education.

Dr. Las-Heras was the Telefónica Chair on "RF Technologies," "ICTs applied to Environment," and "ICTs and Smartcities" at the University of Oviedo from 2005 to 2015. He was a member of the board of directors of the IEEE Spain Section from 2012 to 2015, and he has been a member of the Science, Technology and Innovation Council of Asturias, since 2010.



**Nemat Dolatsha** (S'06) received the M.Sc. degree in electrical engineering from the University of Tehran, Tehran, Iran, in 2009, and the Ph.D. degree from the Swiss Federal Institute of Technology (ETHZ), Zurich, Switzerland, in 2013.

He was a Visiting Scholar with the Center of Integrated Systems (CIS), Stanford University, Stanford, CA, USA, from 2012 to 2013, and joined to this group again in 2014 as a Post-Doctoral Scholar. He is currently a Research Associate with CIS.

His current research interests include high-speed millimeter-wave wireless and wireline links, antennas and phase arrays, energy harvesting for mm-sized sensors, and microwave thermos-acoustic detection and imaging.

Dr. Dolatsha was a recipient of the Best Paper Award at IEEE ICUBW 2013 conference, also the co-recipient of the Best Paper Award at PIERS 2015. He was the co-recipient of the John von Neumann Award of the Systems on Nanoscale Information Fabrics Research Organization.



**Baptiste Grave** received the engineering diploma from the Institut Supérieur d'Électronique et du Numérique, Lille, France, in 2009, and the Ph.D. degree in electrical engineering from Lille 1 University, Villeneuve-d'Ascq, France, in 2013.

He was a Post-Doctoral Researcher with the DC-THz Lab, Stanford University, Stanford, CA, USA, from 2014 to 2016. He is currently a Research Engineer with CEA-LETI, Grenoble, France. His current research interests include mm-wave communication systems and mm-wave IC design for high data-rate communications.



**Mahmoud Sawaby** (S'14) received the M.Sc. degree from Cairo University, Giza, Egypt, in 2014, where he focused on a millimeter-wave imaging system for skin and breast tumor detection. He is currently pursuing the Ph.D. degree in electrical engineering with Stanford University, Stanford, CA, USA.

In 2011 and 2014, he was a part-time Analog Design Engineer with Si-ware systems, where he designed front-ends for bridge interfaces, thermal control loops, and cap-less ADC reference buffers.

His current research interests include mm-Wave systems for high-speed wireless links, and low-power IC designs.

Mr. Sawaby was a recipient of the TGD Best Graduation Project Award in 2011, and the Fairchild Most Unusual Design Award in 2014.



**Amin Arbabian** (S'06–M'12) received the Ph.D. degree in electrical engineering and computer science from the University of California at Berkeley (UC Berkeley), Berkeley, CA, USA, in 2011.

From 2007 and to 2008, he was part of the Initial Engineering Team, Tagarray, Inc., Palo Alto, CA, USA. He was with the Qualcomm's Corporate Research and Development Division, San Diego, CA, USA, in 2010, where he designed circuits for next-generation ultra-low power wireless transceivers. In 2012, he joined Stanford University, Stanford, CA, USA, as an Assistant Professor of electrical engineering, where he is currently a Frederick E. Terman Fellow with School of Engineering. His current research interests include high-frequency systems, medical imaging, Internet-of-Everything devices including wireless power delivery techniques, and medical implants.

Dr. Arbabian was a recipient or co-recipient of the 2016 Stanford University Tau Beta Pi Award for Excellence in Undergraduate Teaching, the 2015 NSF CAREER Award, the 2014 DARPA Young Faculty Award including the Director's Fellowship in 2016, the 2013 Hellman Faculty Scholarship, the 2010–2011, 2014–2015, and 2016–2017 Qualcomm Innovation fellowships, and best paper awards at the 2016 IEEE Conference on Biomedical Wireless Technologies, Networks, and Sensing Systems, 2014 IEEE VLSI Circuits symposium, 2013 IEEE International Conference on Ultra-Wideband (ICUWB), the 2010 IEEE Jack Kilby Award for Outstanding Student Paper at the International Solid-State Circuits Conference, and two time second place best student paper awards at 2008 and 2011 RFIC symposiums. He currently serves on the steering committee of RFIC Symposium, the technical program committees of RFIC symposium, ESSCIRC, and VLSI Circuits Symposium, and as an Associate Editor of the IEEE SOLID-STATE CIRCUITS LETTERS and the IEEE JOURNAL OF ELECTROMAGNETICS, RF AND MICROWAVES IN MEDICINE AND BIOLOGY.